J Nanopart Res (2022) 24:105
https://doi.org/10.1007/s11051-022-05493-5

RESEARCH PAPER

Effects of chlorine particle concentration on the human airway

Fifi N. M. Elwekeel · Xinguang Cui · Antar M. M. Abdala

Received: 29 December 2021 / Accepted: 11 May 2022
© The Author(s) 2022

Abstract For COVID-19, chlorine has lately been utilised as a home disinfectant. Given that chlorine is hazardous to the human airway, the current research investigates the effects of chlorine mass fraction and droplet size on the human airway. The effects are investigated at chlorine mass ratios of 2% (24 ppm), 10% (120 ppm), 15% (180 ppm), and 20% (240 ppm), as well as chlorine particle diameters of 10 nm, 20 nm, 30 nm, and 50 nm, and three inhalation rates (15 l/min, 30 l/min, and 60 l/min). The results reveal that when the chlorine mass fraction is 2% and the inhalation rate is low, the chlorine volume fraction decreases. Furthermore, at 2% chlorine and a rapid breathing rate, chlorine particles are accelerated to escape into the lungs.

Keywords Environmental and health effects · Chlorine particles · Human airway · COVID-19

F. N. M. Elwekeel
Faculty of Industrial Education, Helwan University, Cairo, Egypt
e-mail: fifinew2000@yahoo.com

X. Cui
School of Aerospace Engineering, Huazhong Science and Technology University, Wuhan, China
e-mail: xinguang_cui@hust.edu.cn

A. M. M. Abdala (✉)
Faculty of Engineering, Matareya Branch, Helwan University, Cairo 11718, Egypt
e-mail: antar451@yahoo.com

Introduction

There are many different types of environmental aerosols that are inhaled and transported through the human airways. These particles may come into contact with the airway surface and cause a harmful reaction. The relation between aerosol particle sizes and bronchial illnesses has been studied extensively. Underground miners have been found to get lung cancer as a result of their exposure to ultrafine particles (less than 200 nm) (Cheng and Swift 2016). Nanoparticles in the air were more damaging and hazardous, particularly to the elderly and those with respiratory disorders (Frampton 2001; Donaldson et al. 2000; Oberdorster 2001; Kumar and Goel 2016). Underwood (Underwood 2017) and Chen et al. (Chen et al. 2017) demonstrated that there was a relation between ill health and a polluted environment.

Over the last 25 years, other research have looked into the health dangers of aerosols and the causes of early death (ICRP 1994; Cohen et al. 2017; Heal et al. 2012; Lelieveld et al. 2015). These particles have a diameter of less than 0.1 μm and contributed to air pollution. Fuel exhaust (5 to 500 nm) (Kumar and Goel 2016), smoke (140 to 500 nm) (Kittelson 1998; Bernstein 2004), and radionuclides (2 to 200 nm) (Keith 1982) are all contributors of this aerosol. The capacity of these nanoparticles to deposit in the airway was explored in these studies. Age, sex, and health status all influenced the percentage of these particles deposited (Kim and Jaques 2004; Horemans

Published online: 20 May 2022

et al. 2012; Chalupa et al. 2004). For example, with a particle size of 0.04 nm, females had a higher percentage of deposition than males.

Other studies (Kan et al. 2007; Chen et al. 2012, 2011; Meng et al. 2013; Breitner et al. 2011; Li et al. 2016) looked at how much particle matter was deposited in people's lungs in the most polluted cities. People with heart disease were more likely to die in a contaminated environment with particles ranging in size from 30 to 100 nm, according to these research.

The majority of earlier investigations focused on nanoparticle deposition in the airway caused by fuel vapour and cigarette smoke. However, disinfectants are increasingly critical for coronavirus sterilisation. Chlorine is one of the most well-known disinfectants, and it is used in various concentrations, because chlorine gas is a hazardous gas that induces respiratory symptoms at 15 ppm and can be deadly at 430 ppm within 30 min (Chauhan et al. 2008). Chlorine has a variety of toxicity in the lungs, as seen in Fig. 1. When it comes into contact with mucosal surfaces and airways, it produces various acidic forms and a range of highly reactive oxidants (White and Martin 2010). As a result, the quantitative deposition of chlorine particles in the airway will be examined in this work. In addition, the effects of various chlorine concentrations and particle sizes will be described in this study.

Methods

Geometry

Figure 2 depicts the oral airway configuration. The mouth cavity, pharynx, larynx, and trachea are all part of it. Cheng et al. (Cheng et al. 1997) investigated the oral airway configuration experimentally, and the 3D oral airway structural mesh is generated using the ICME Ansys software. The grid independence for airways was tested by Zhang and Kleinstreuer (Zhang and Kleinstreuer 2004) and Cui and Gutheil (Cui and Gutheil 2017, 2018); they chose 740,000 cells. The grid size will be examined at one million cells in the current study. The refine mesh is on the wall in order to capture particle deposition and keep Y^+ below one (Fig. 2b).

Governing equations

The governing equations will be utilised to explore the flow in the human airway, and ANSYS CFX will be used to solve these equations. The three flow rates employed in low, medium, and high breathing are 15, 30, and 60 l/min (Zhang and Kleinstreuer 2004). The continuous fluid is ideal air, while the discreated fluid is chlorine particles. The continuous fluid enters at a constant velocity (0.8, 1.6,

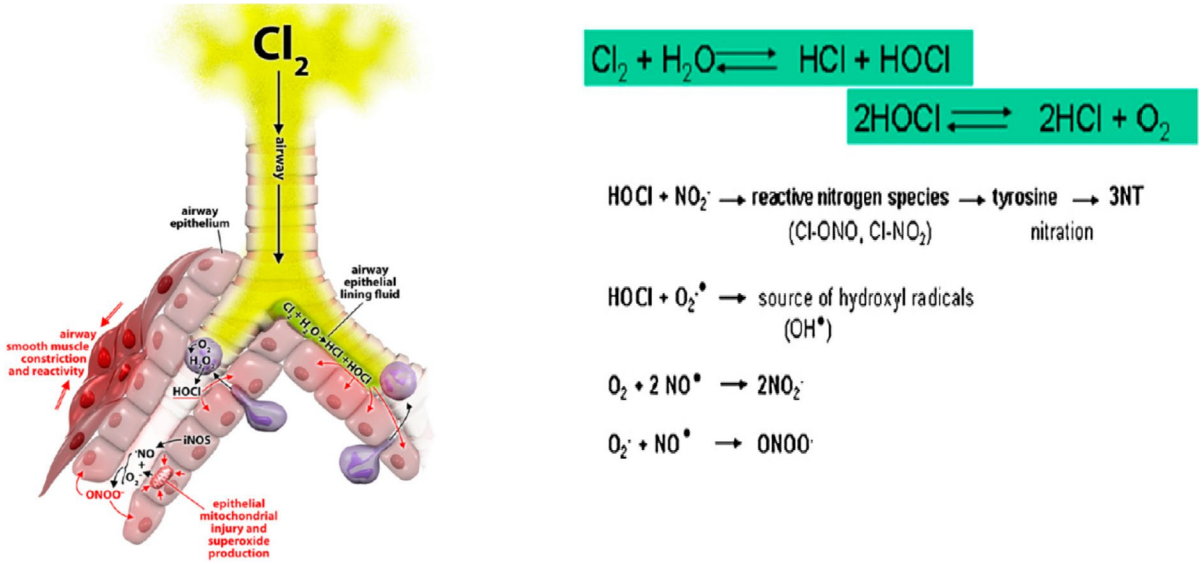

Fig. 1 Chlorine reactions in the airway at chlorine inhalation (White and Martin 2010)

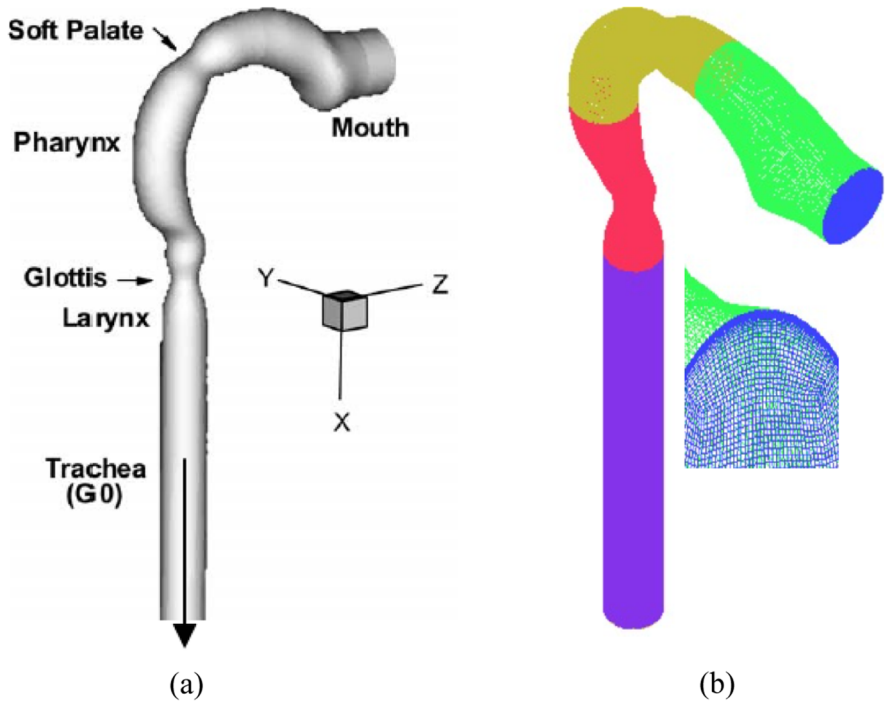

Fig. 2 Geometry of the upper airway (Zhang and Kleinstreuer 2004): (**a**) computation domain, (**b**) mesh grid

and 3.2 m/s). Isothermal temperature (300 K), subsonic flow, 1-atm relative pressure, and low turbulence intensity characterise the flow regime. The exit pressure is zero, and the airway walls are considered to be no slip condition. The inlet velocity of the discreated fluid is set to that of the continuous fluid, and 10,000 chlorine particles (Cui and Gutheil 2017) are uniformly injected into the inlet. The mass ratio of chlorine 2%, 10%, 15%, and 20% is employed with mean particle diameters of 10 nm, 20 nm, 30 nm, and 50 nm, respectively (Zhang and Kleinstreuer 2004).

In the absence of gravity, the Euler-Euler method is used to model particle motion. The following equations are used to compute the transit of chlorine particles in breathed air.

Continuous fluid

Ideal air is a continuous fluid that flows into the airway with chlorine particles. This study is conducted under steady-state, incompressible, and isothermal conditions.

Continuity:

$$\frac{\partial u_i}{x_i} = 0 \tag{1}$$

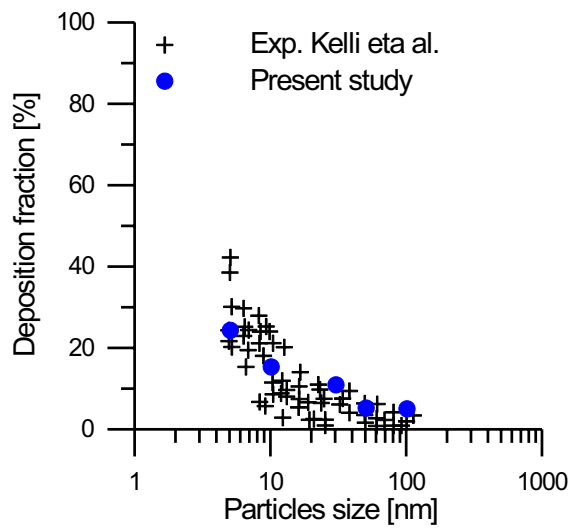

Fig. 3 Relation between deposition fraction and particles size

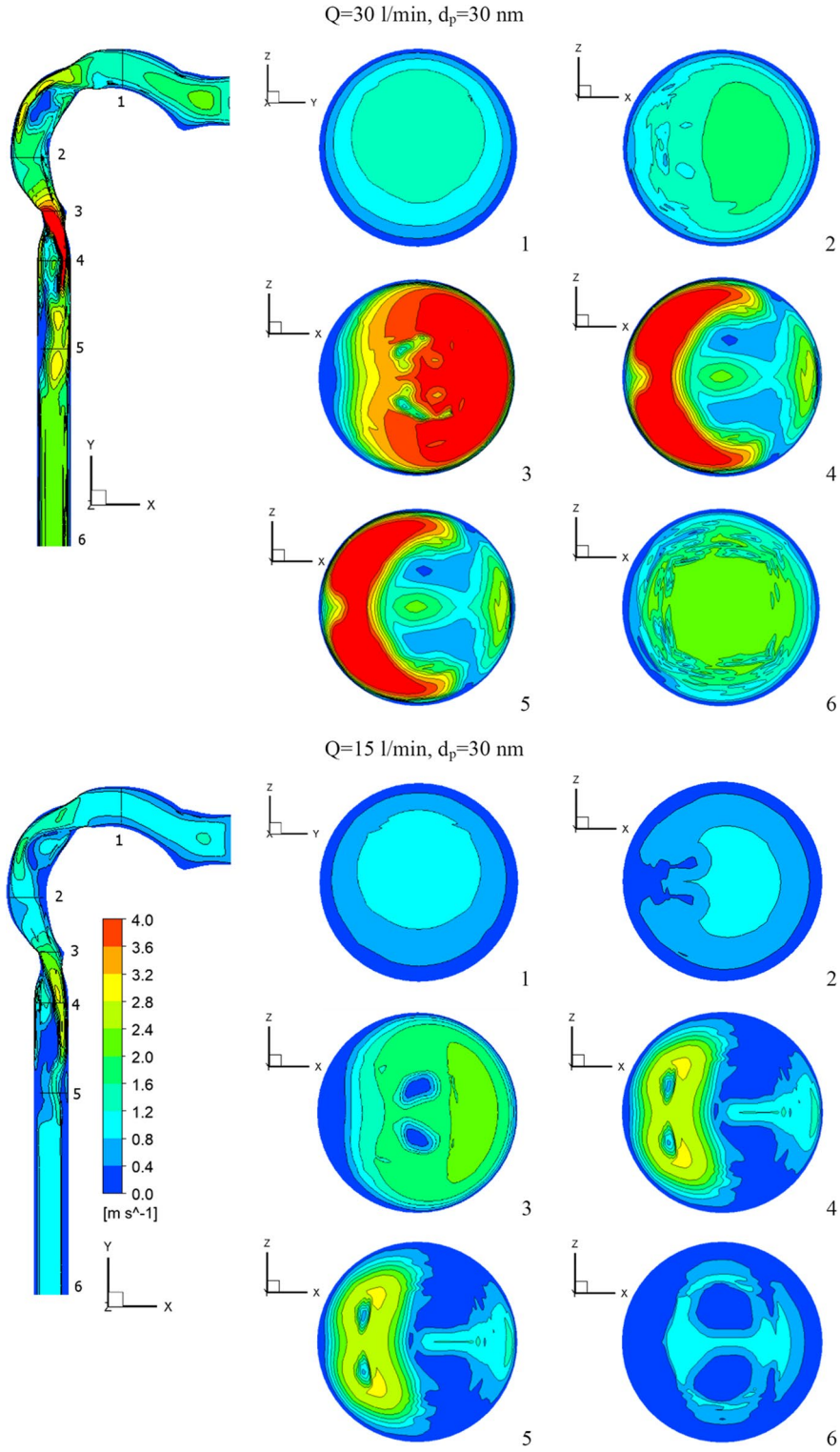

Fig.4 Velocity of chlorine particles in the airway

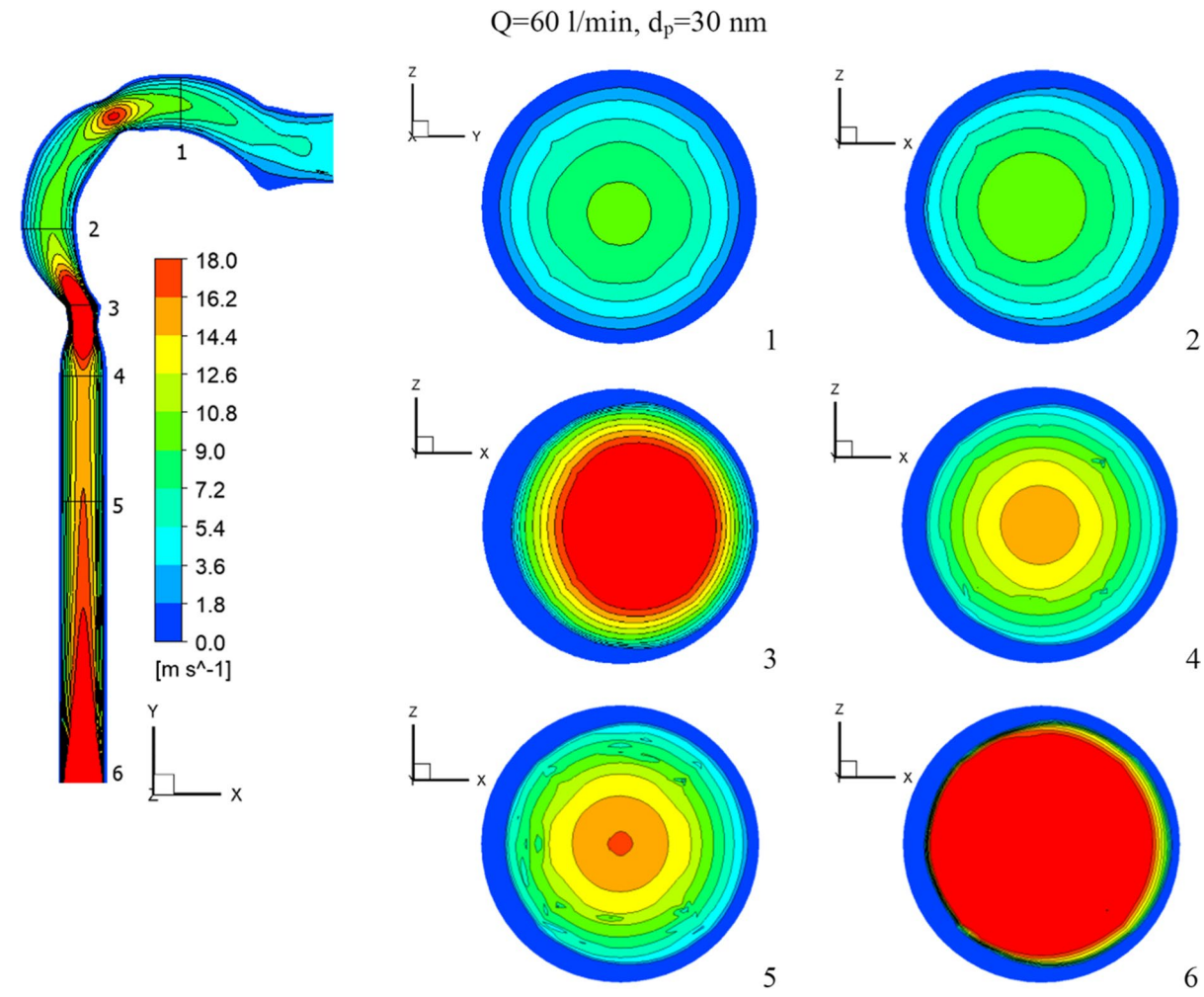

Fig.4 (continued)

Momentum:

$$u_j \frac{\partial u_i}{\partial x_j} = -\frac{1}{\rho}\frac{\partial p}{\partial x_i} + v\frac{\partial^2 u_i}{\partial x_j \partial x_j} \tag{2}$$

where $i, j = 1$, 2, and 3. u_i is the air velocities in x, y, and z directions. $p, \rho,$ and v are the pressure, the density, and the kinematic viscosity of air, respectively.

Discrete fluid (nanoparticles)

The mass transport equation of nanoparticles is (Friedlander 2000):

$$\frac{\partial (u_j C)}{\partial x_j} = \frac{\partial}{\partial x_j}\left(D\frac{\partial C}{\partial x_j}\right) \tag{3}$$

C and D are the concentration and the effective diffusion coefficient of nanoparticles, respectively. The effective diffusion coefficient of nanoparticle can be calculated as (Cheng et al. 1988):

$$D = \frac{\left(K_B T C_{\text{slip}}\right)}{\left(3\pi\mu d_p\right)} \tag{4}$$

$$C_{\text{slip}} = 1 + \frac{2\lambda_m}{d_p}\left[1.142 + 0.058e^{\left(-0.999\frac{d_p}{2\lambda_m}\right)}\right] \tag{5}$$

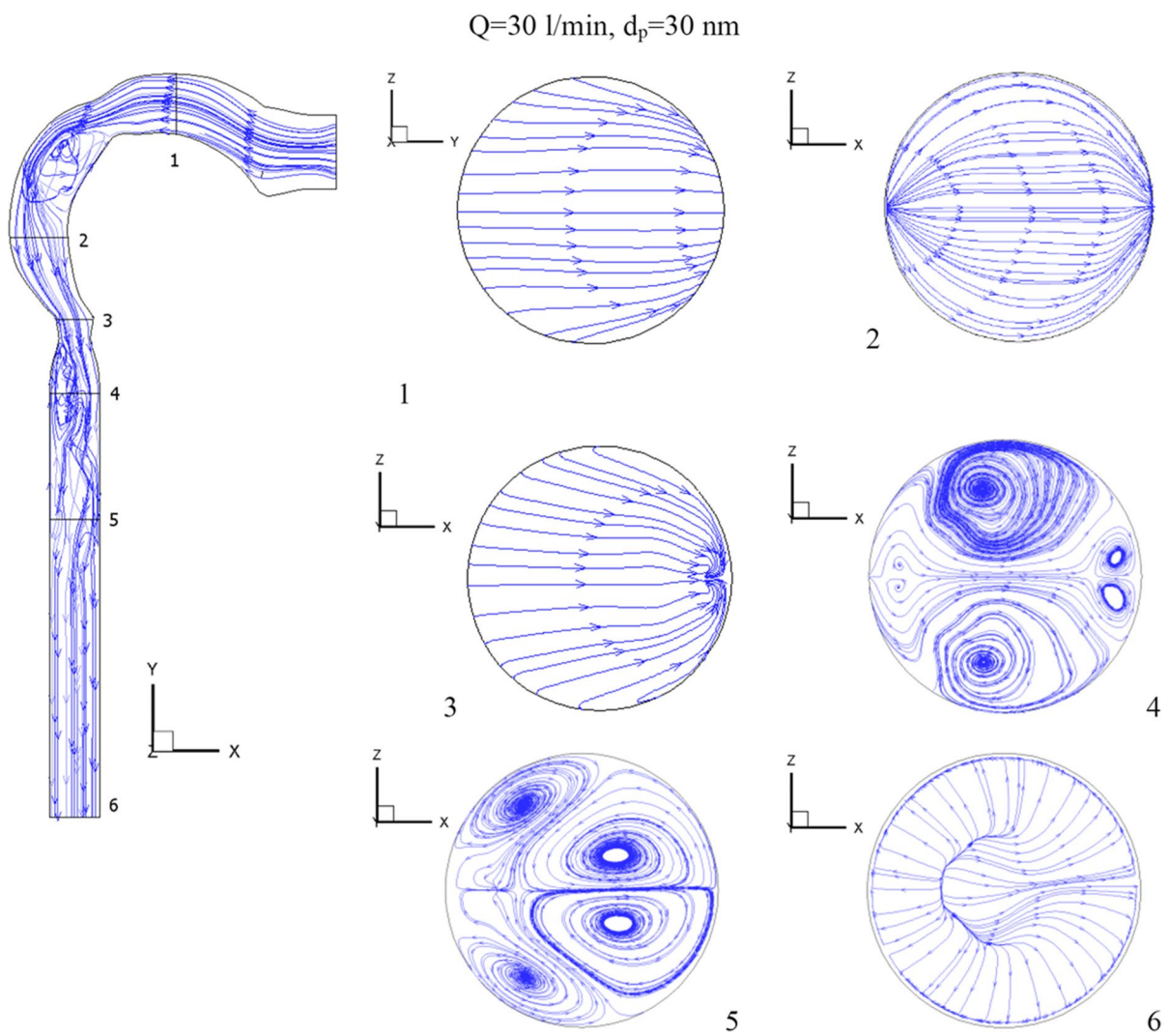

Fig. 5 Velocity streamline in the airway

K_B, T, C_{slip}, and λ_m are the Boltzmann constant, the air absolute temperature, the Cunningham correction, and the mean free path in the air, respectively.

The nanoparticle deposition fraction is the ratio of the mass deposited on the wall to the inlet mass flow rate, which can be calculated as (Ghalati et al. 2012):

$$\left(DF_i\right)_{\text{nanoparticles}} = \frac{\dot{m}_{w,i}}{\dot{m}_{in}} \tag{6}$$

The total mass deposition $\dot{m}_{w,i}$ can be written as:

$$\dot{m}_{w,i} = \sum_{j=1}^{N} -\rho A_j D \frac{\partial C}{\partial n}\bigg|_{w,j} \tag{7}$$

N is the number of cells closest to the walls in one certain region, n is the normal direction to the wall, and A_j is the face area of each cell next to the walls in region i.

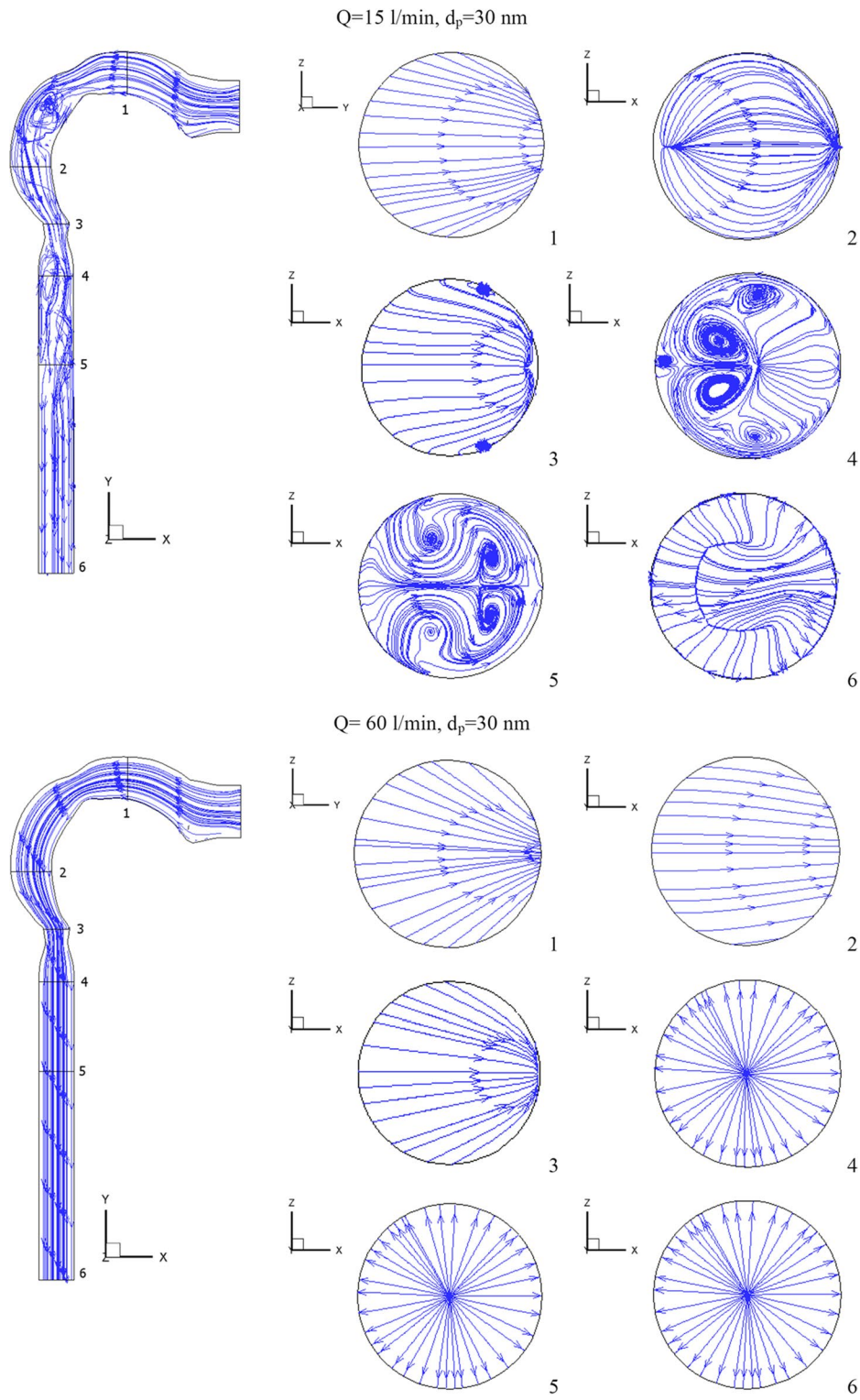

Fig. 5 (continued)

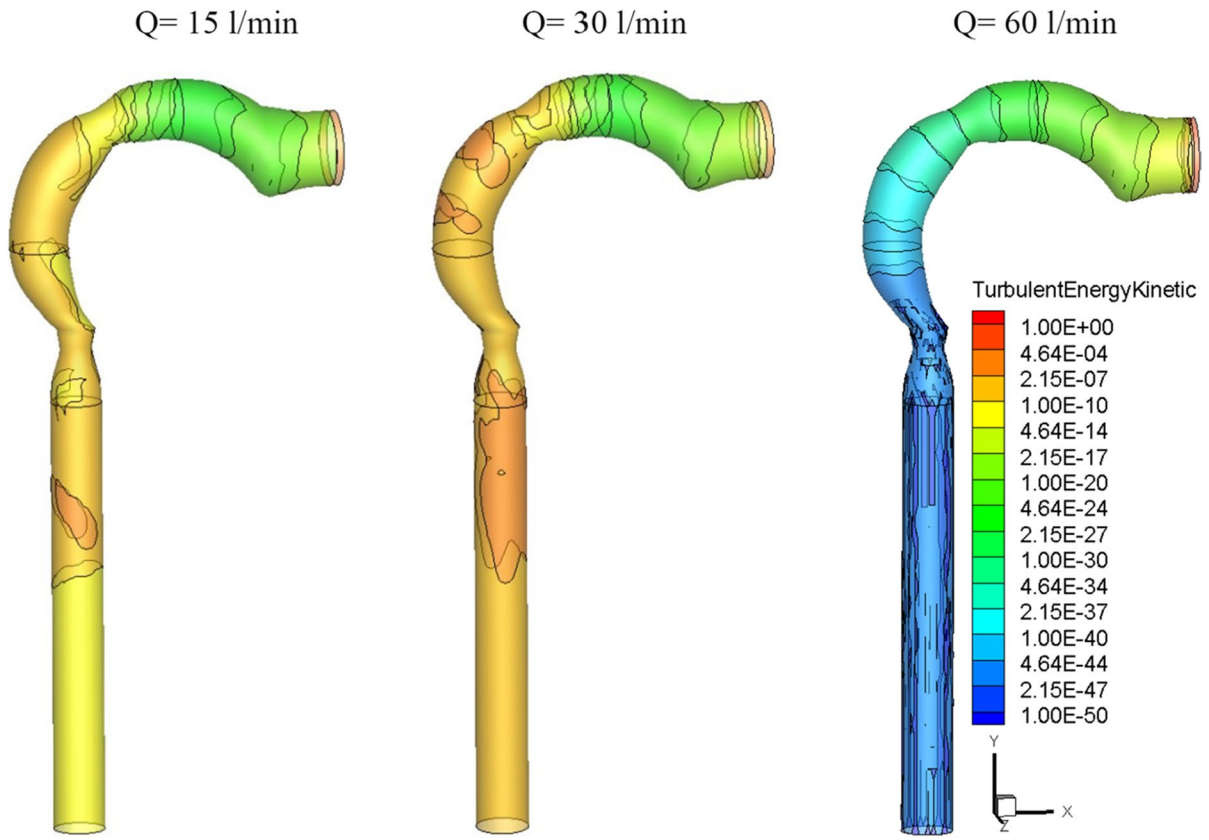

Fig. 6 Turbulence kinetic energy with different inhalation rates and $d_p = 30$ nm [m^2/s^2]

Validation

To validate the numerical model with experimental results, the low Reynolds number K-ω model was adopted. Several investigations (Zhang and Kleinstreuer 2004, 2003) have identified this model as well. This model has been proved to be a viable method for capturing velocity profiles and kinetic energy disturbance of transitional flows in the upper airways' narrow tubes. For the experimental investigation (Kelly et al. 2004) and numerical data, Fig. 3 depicts the relationship between deposition fraction and particle size. Verification is carried out at particle sizes ranging from 2 to 100 nm, with a mass fraction of 2% (24 ppm) and a flow rate of 15 l/min. The K-ω model is congruent with the experimental model in this figure; hence, it can be used in this investigation. RMS residuals of $1 * 10^{-5}$ are used as convergence criterion.

Results

Effect of respiratory flow rates at chlorine mass fraction 2%

The flow of the chlorine/air mixture into the airway will be shown in this section. Inhalation rates are 15 l/min, 30 l/min, and 60 l/min. The chlorine particles have a diameter of 30 nm and a mass fraction of 2% chlorine (24 ppm). Figure 4 depicts the chlorine velocity at various locations and inhalation flow rates. With higher flow rates, the chlorine velocities increase. The velocity increases in the pharynx/larynx for low and medium inhalation rates, and the maximal location shifts due to centrifugal force (see cross-Sects. 3 and 4). The velocity is more uniform with a high inhalation rate ($Q = 60$ l/min), and the maximum velocity is in the

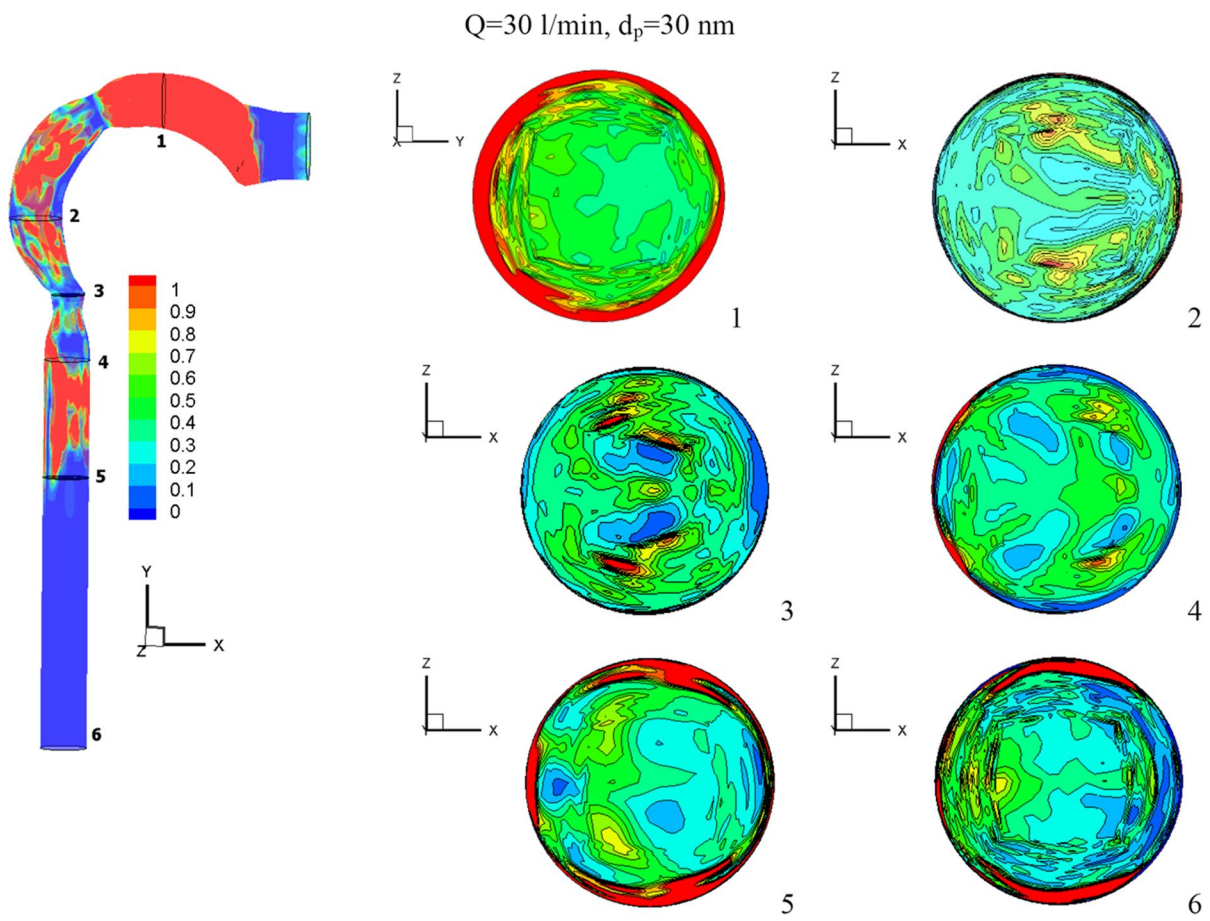

Fig. 7 The distribution of chlorine volume fraction

center. As seen in Fig. 5, at inhalation flow rates of 15 and 30 l/min, the separation at the airway wall rises. As illustrated in cross-Sect. 4, changing the laryngeal cross-section causes secondary flow. The highest velocity is achieved at the center at a high inhalation flow rate of 60 l/min because the pressure gradient is driven by centrifugal force (Kleinstreuer and Zhang 2003).

Figures 4 and 5 further show that the Dean number has an impact on inhalation flow rates of 15 and 30 l/min. When the rate of breathing increases, the Dean number rises, causing a separation as the fluid flows into the outer wall. The greater flow rate combined with the shift in airway cross-section overcomes the adverse pressure gradient and the production of vortices at a 60 l/min inhalation rate. The turbulent kinetic energy for low, medium, and high inhalation rates is shown in Fig. 6. At $Q=15$ l/min and $Q=30$ l/min, turbulence strength is minimal in the oral cavity but increases in the pharynx, larynx, and trachea. The uniform velocity of a higher inhalation flow rate leads to a decrease in eddy generation and a reduction in turbulent kinetic energy.

Figure 7 shows the chlorine volume fraction for $Q=15$ l/min, $Q=30$ l/min, and $Q=60$ l/min at particle diameter of 30 nm and mass fraction 2% (24 ppm). When the rate of inhalation rises, the volume fraction of chlorine drops. Near low inhalation (15 l/min), the chlorine concentration is spread throughout the airway, with a high value at the exit airway (cross-Sect. 6). The chlorine particles are clustered towards the wall and at their highest concentration in the mouth cavity for medium inhalation (30 l/min). The minimal velocity at the wall (see Fig. 6) results in less convection mass transfer and a lower chlorine volume percentage (Zhang and Kleinstreuer 2004).

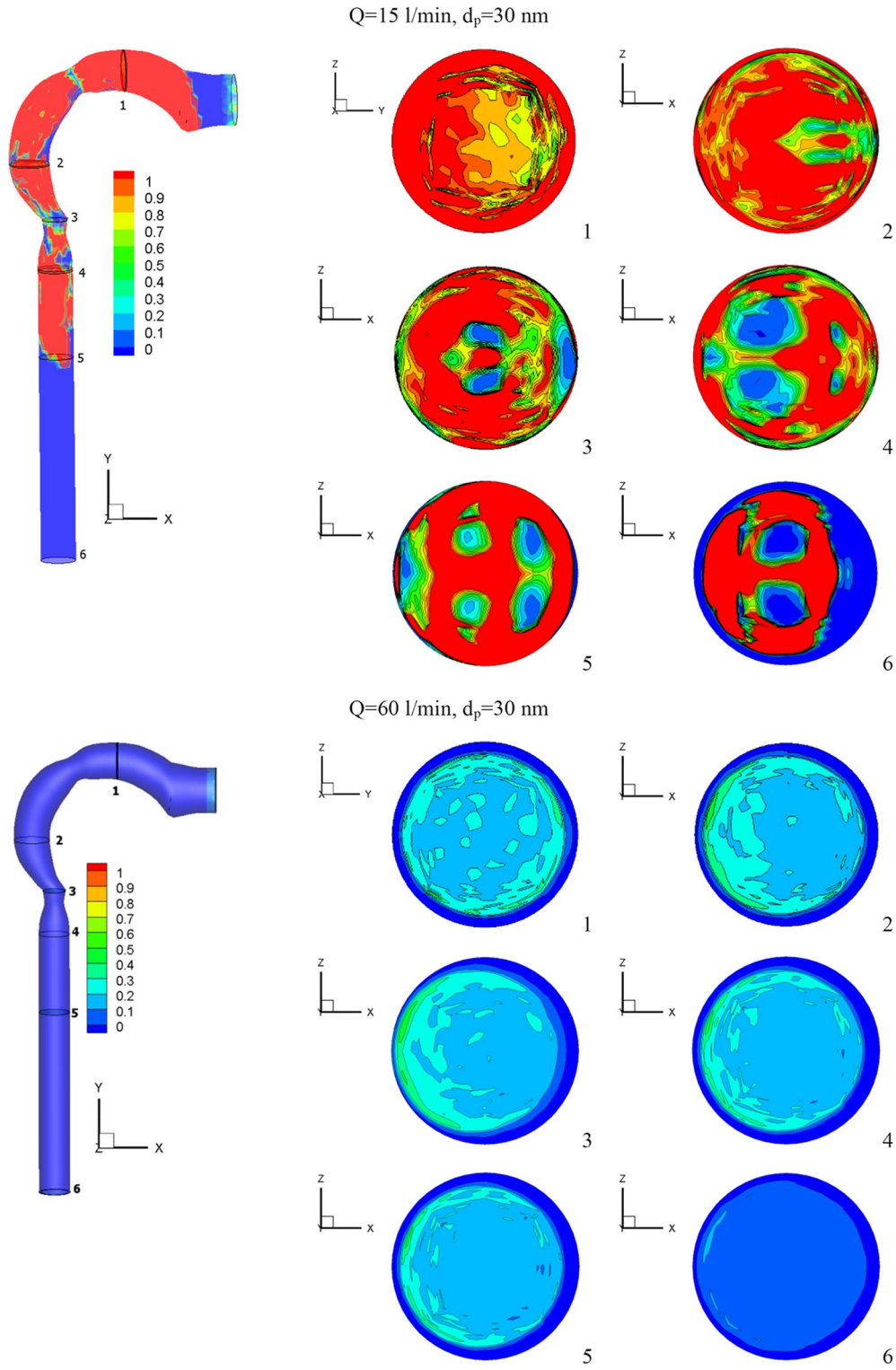

Fig. 7 (continued)

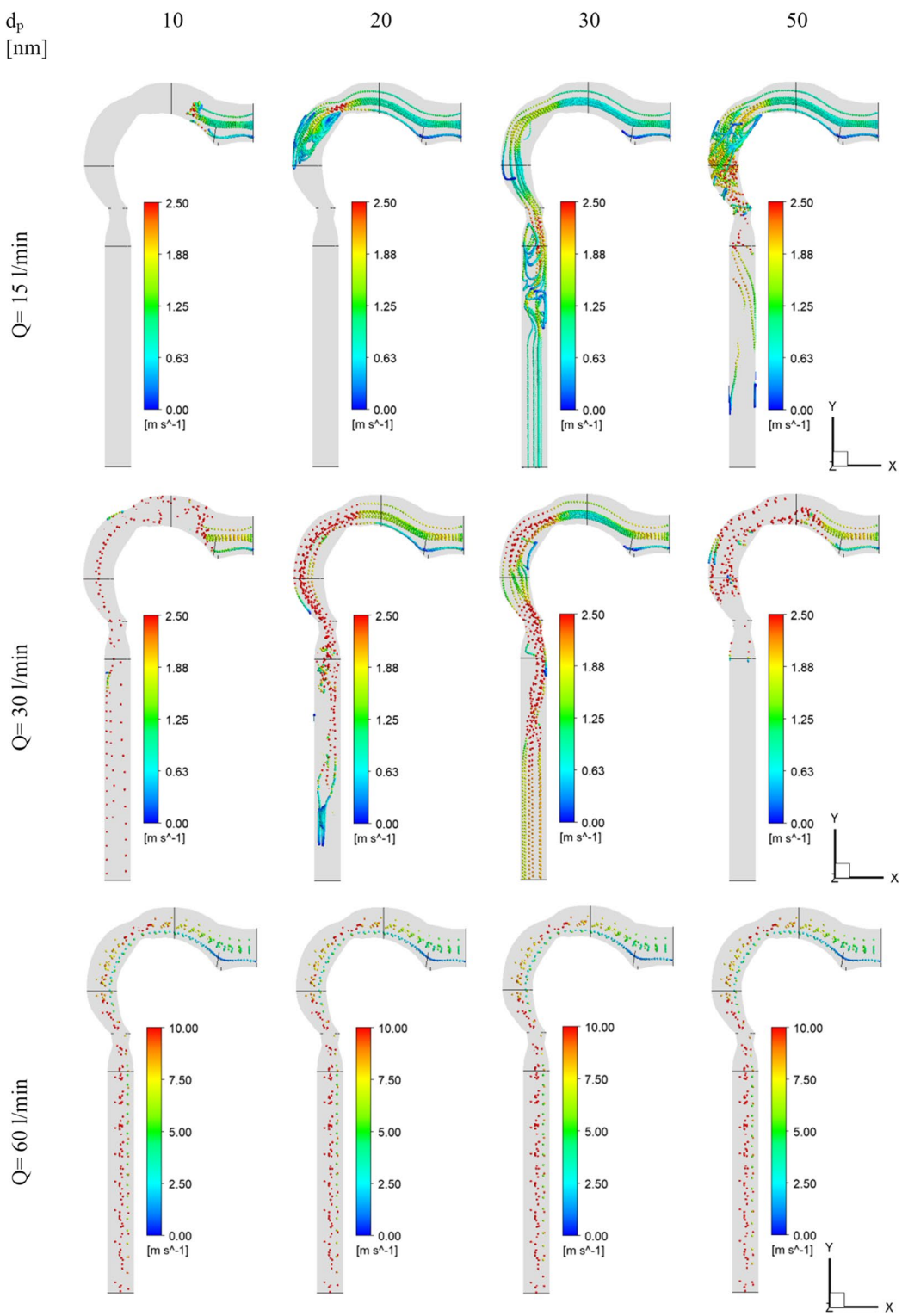

Fig. 8 Chlorine velocity at different inhalation rates

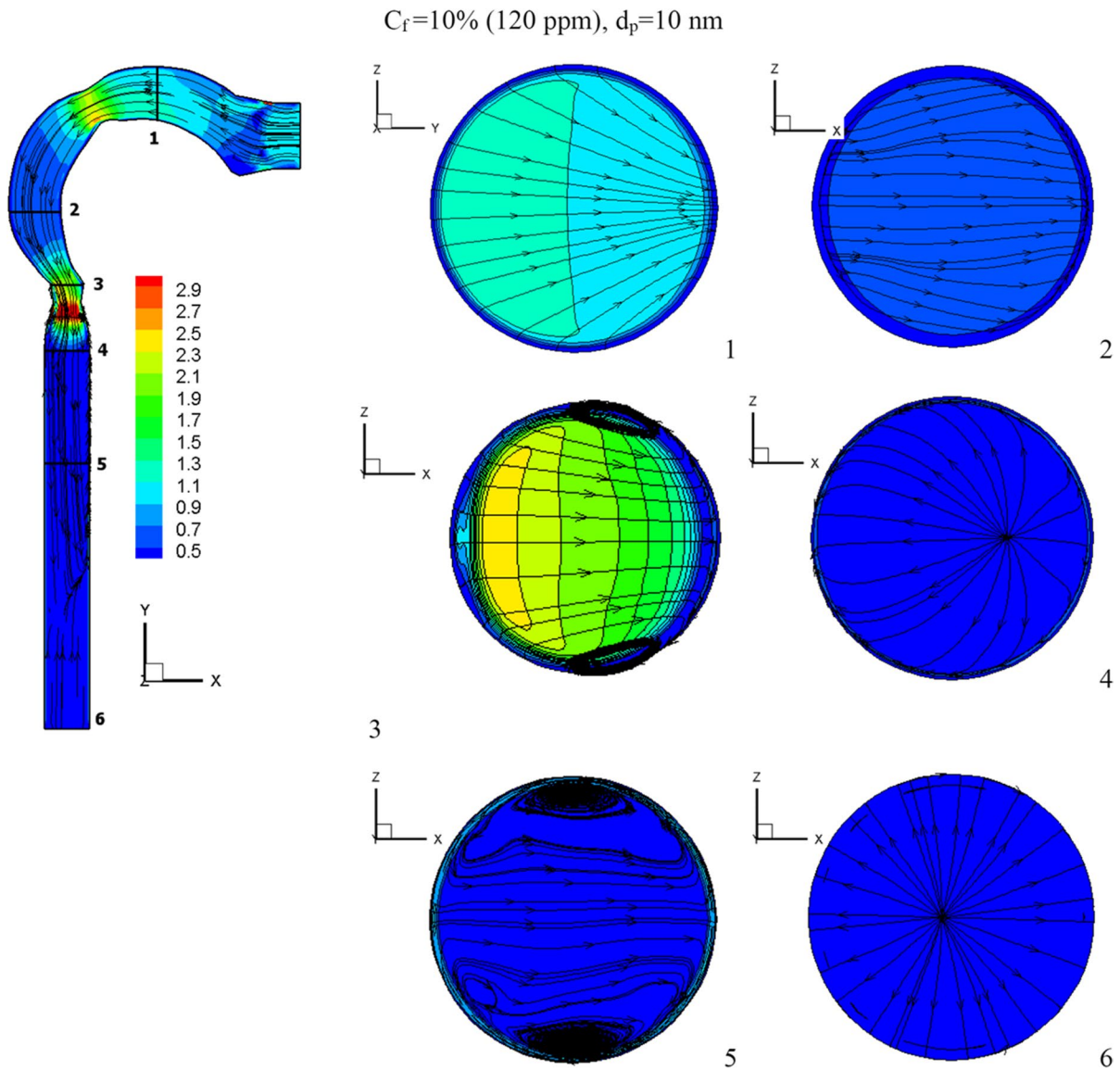

Fig. 9 Velocity contour at varied chlorine mass fractions

Effect of chlorine particle diameter

Figure 8 depicts the average velocity of particles at various particle sizes and flow rates. The velocity of the particles drops and reaches the maximum transmission distance in the mouth cavity at a respiratory flow rate of 15 l/min, a particle size of 10 nm, and a chlorine mass fraction of 2% (24 ppm). With a lower respiratory flow rate, chlorine particles have a lower velocity, which causes more vortices in the airway. Chlorine particles are kept out of the bronchial tube by these vortices. Particles of 50 nm cause higher pharyngeal disruptions at low respiratory flow rates (15 l/min) and intermediate respiratory flow rates (30 l/min). This is due to the particles gaining a lot of kinetic energy as the cross-section of the airway changes. The particles are accelerated to escape into the bronchial tubes at a high respiratory flow rate of 60 l/min. At the pharynx and larynx inlets, the particles have a high velocity.

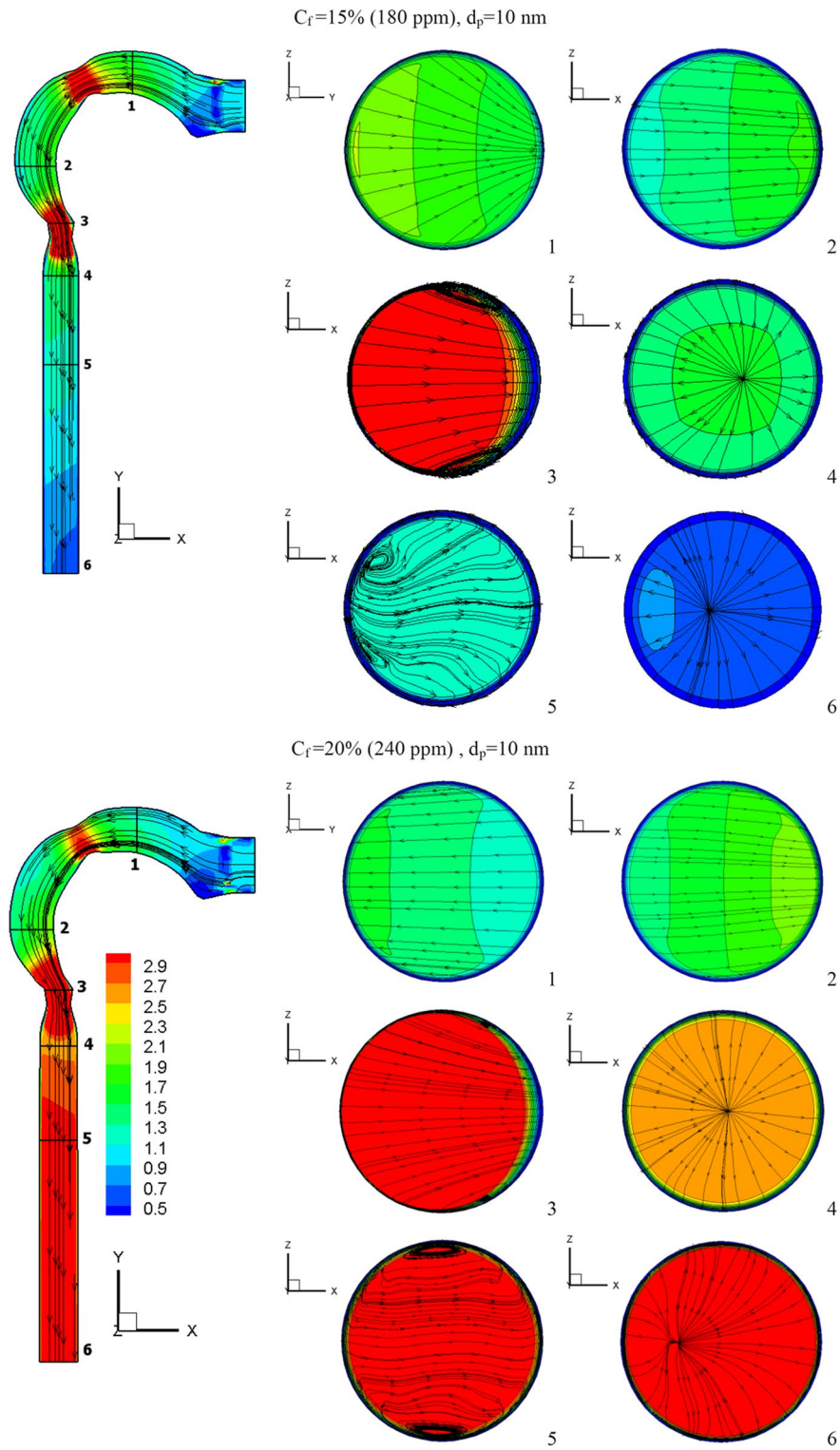

Fig. 9 (continued)

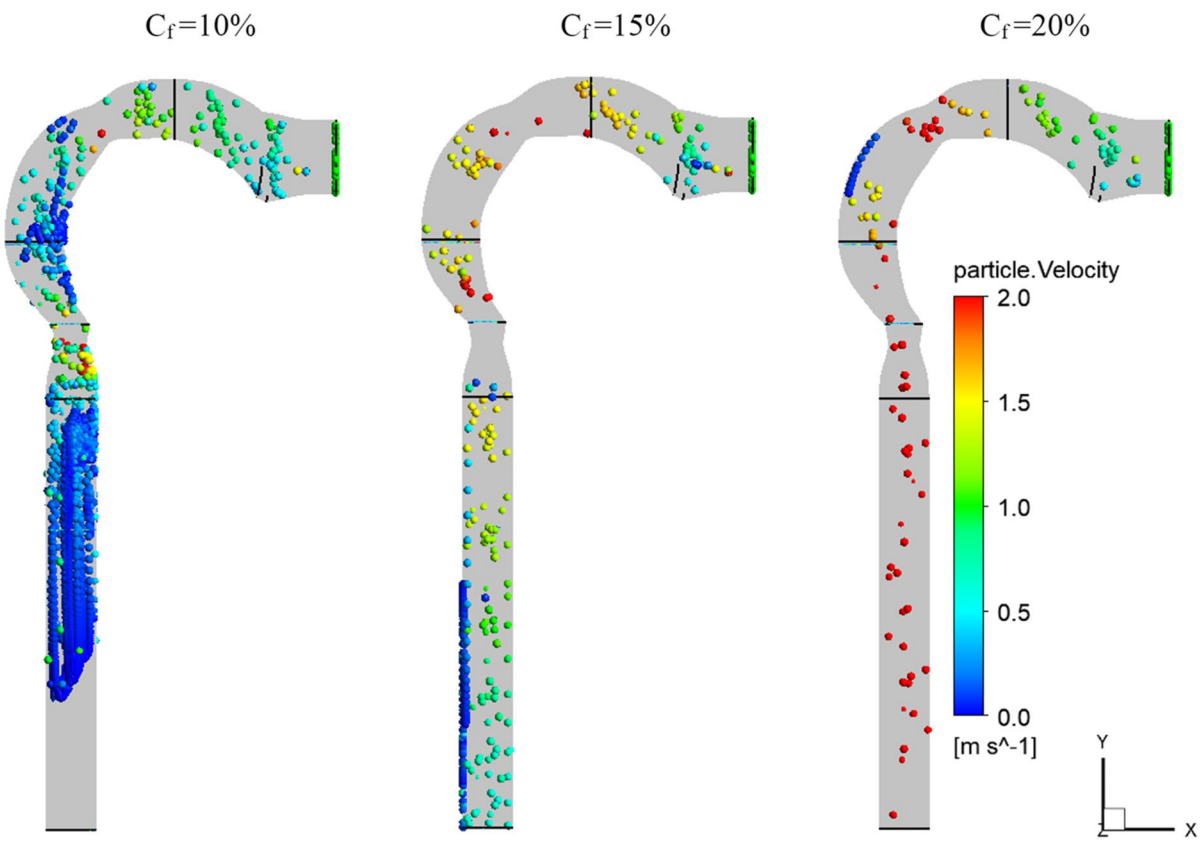

Fig. 10 Chlorine velocity at different chlorine mass fractions and $d_p = 10$ nm

Effects of chlorine mass fraction

This section will explain how chlorine particles behave in the human airway when the mass fraction of chlorine is 10% (120 ppm), 15% (180 ppm), and 20% (240 ppm). The streamline velocity and velocity contours are shown in Fig. 9. The effects of chlorine mass fraction at a diameter of 10-nm chlorine particles and a flow rate of 15 l/min are shown in this diagram. Increased chlorine mass fraction improves velocity while reducing vortex generation. As the chlorine mass diminishes, the chlorine particles become more concentrated in the trachea, resulting in the production of additional vortices, as seen in cross-Sect. 5. As seen in Fig. 10, the high fraction of chlorine mass creates a high velocity of chlorine particles. By raising the mass fraction of chlorine, the chlorine particles accelerate the flow of liquid. The average velocities for the chlorine mass fractions of 20%, 15%, and 10% at the exit of the airway are 2.7 m/s, 0.62 m/s, and 0.31 m/s, respectively.

The effects of chlorine mass fractions are demonstrated in Fig. 11 at a low inhalation rate of 15 l/min, with mass fractions of 10%, 15%, and 20%, and the chlorine particle diameter is 10 nm. The volumetric percentage of chlorine in the airway with varying chlorine mass fractions is shown in Fig. 11. The mass fraction of chlorine is inversely related to the volume fraction. The chlorine volume fraction concentration varies in different parts of the airway. Because chlorine particles are more stable in the airway with a mass fraction of 10% chlorine, the maximum chlorine volume is attained at cross-Sects. 1 to 5. At a 10% chlorine volume fraction, the deposition of chlorine particles is high because the particles have a decreased velocity, which aids deposition (see Fig. 10). On the other hand, chlorine particles escape into the bronchial airways at 15% and 20% chlorine concentrations.

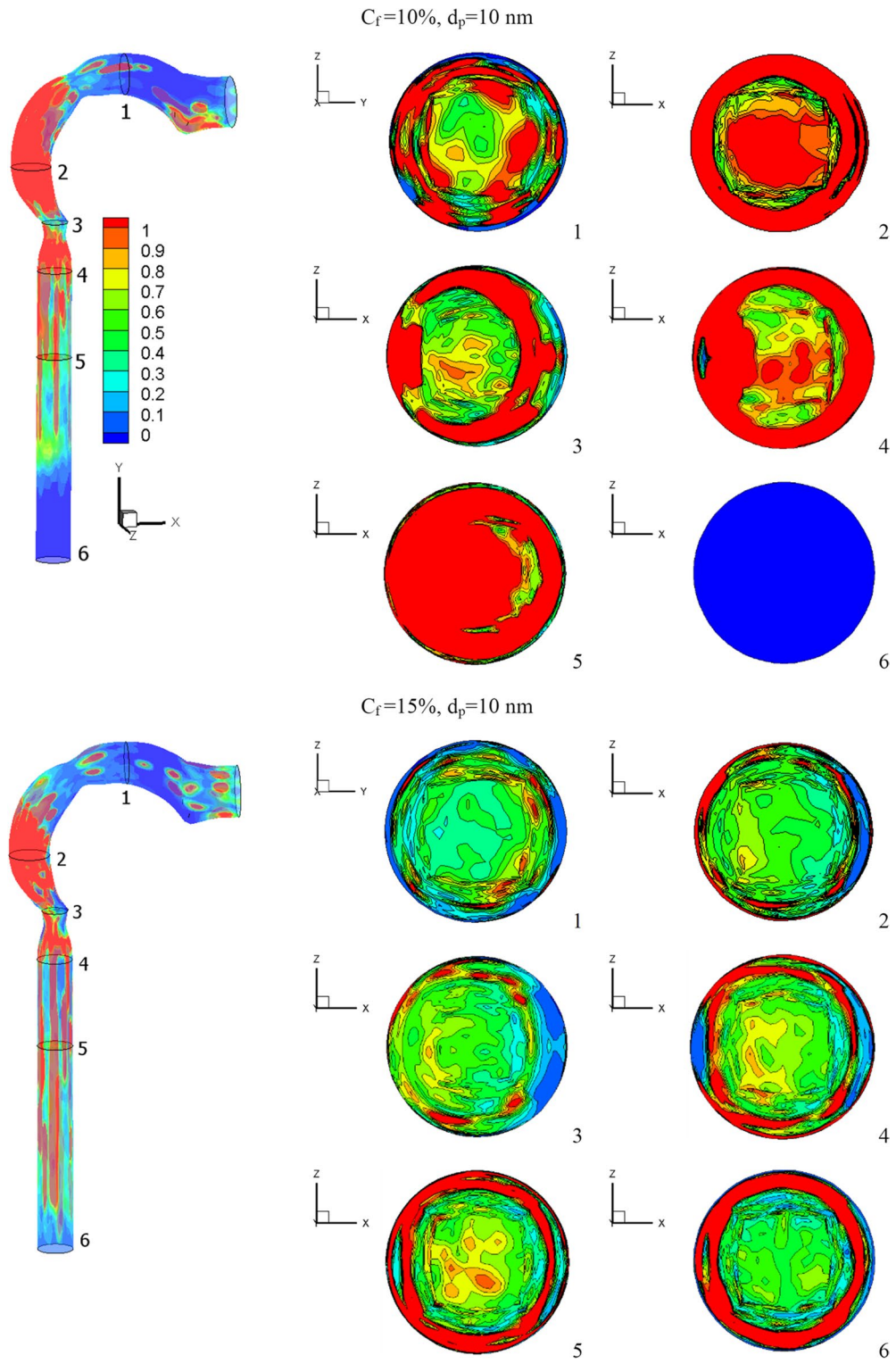

Fig. 11 Volume fraction of chlorine at different chlorine mass fractions

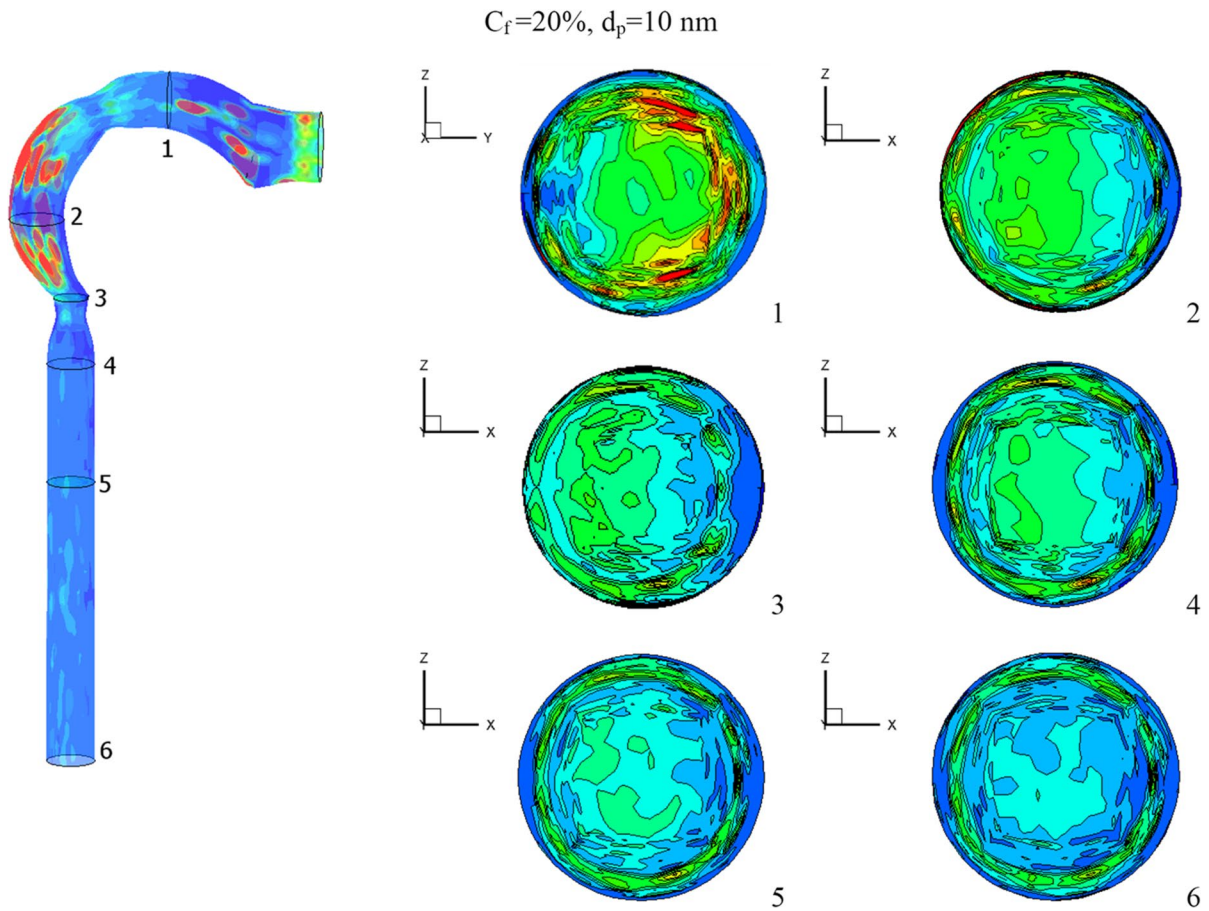

Fig. 11 (continued)

Figure 12 depicts the impact of chlorine mass fraction on turbulent kinetic energy. The mouth cavity has a high value for turbulent kinetic energy. As can be seen, an increase in chlorine particles increases turbulent kinetic energy, particularly at the airway exits (that is matched to Fig. 10). Because chlorine particles adhere to the airway wall, the turbulent kinetic energy near the outer wall of the airway is at its lowest. The average turbulent kinetic energy at the airway exit is 14.4% and 2.2% higher at 20% chlorine than it is at 10% and 15% chlorine, respectively.

Figure 13 describes the relation between chlorine particle deposition efficiency and chlorine mass fraction at various inhalation flow rates. The mass fraction of chlorine has an inverse relationship with deposition efficiency, but the mass fraction of chlorine has a direct relationship with deposition efficiency. This is due to chlorine's high density, which increases centrifugal force as the bulk of chlorine increases, speeding up the particles' exit from the airway. In comparison to $Q=15$ l/min, the deposition efficiency of $Q=60$ l/min and $Q=30$ l/min rises by around 21.8% and 4.1% at a chlorine mass fraction of 20%.

Conclusions

The effects of chlorine particles on human airways are investigated in this study. The airway is tested using different chlorine mass fractions (2%, 10%, 15%, and 20%), different chlorine diameters (10 nm, 20 nm, 30 nm, and 50 nm), and three different inhalation rates (15 l/min, 30 l/min, and 60 l/min). The following is a summary of the research:

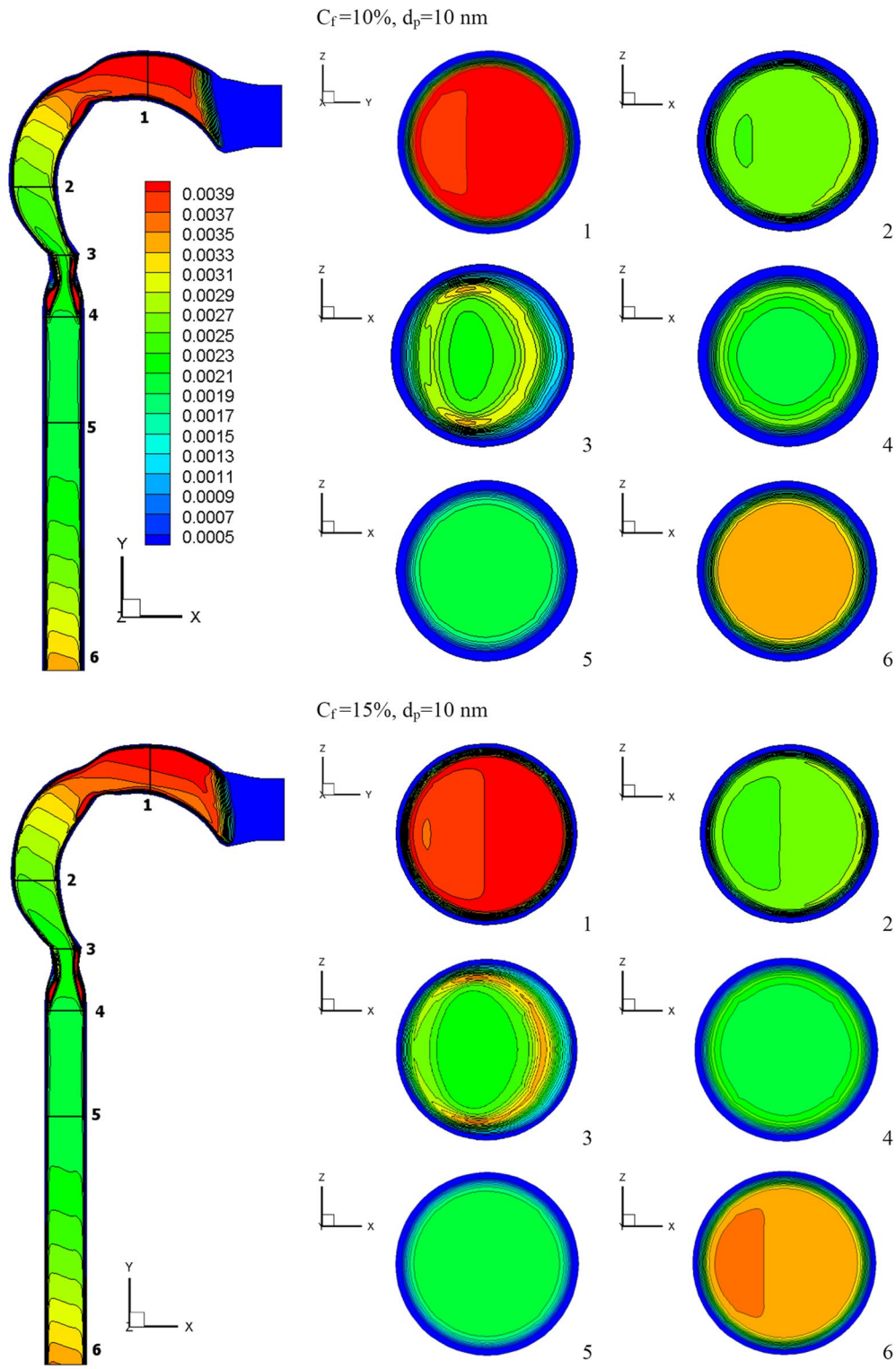

Fig. 12 Turbulent kinetic energy at $d_p = 10$ nm [m^2/s^2]

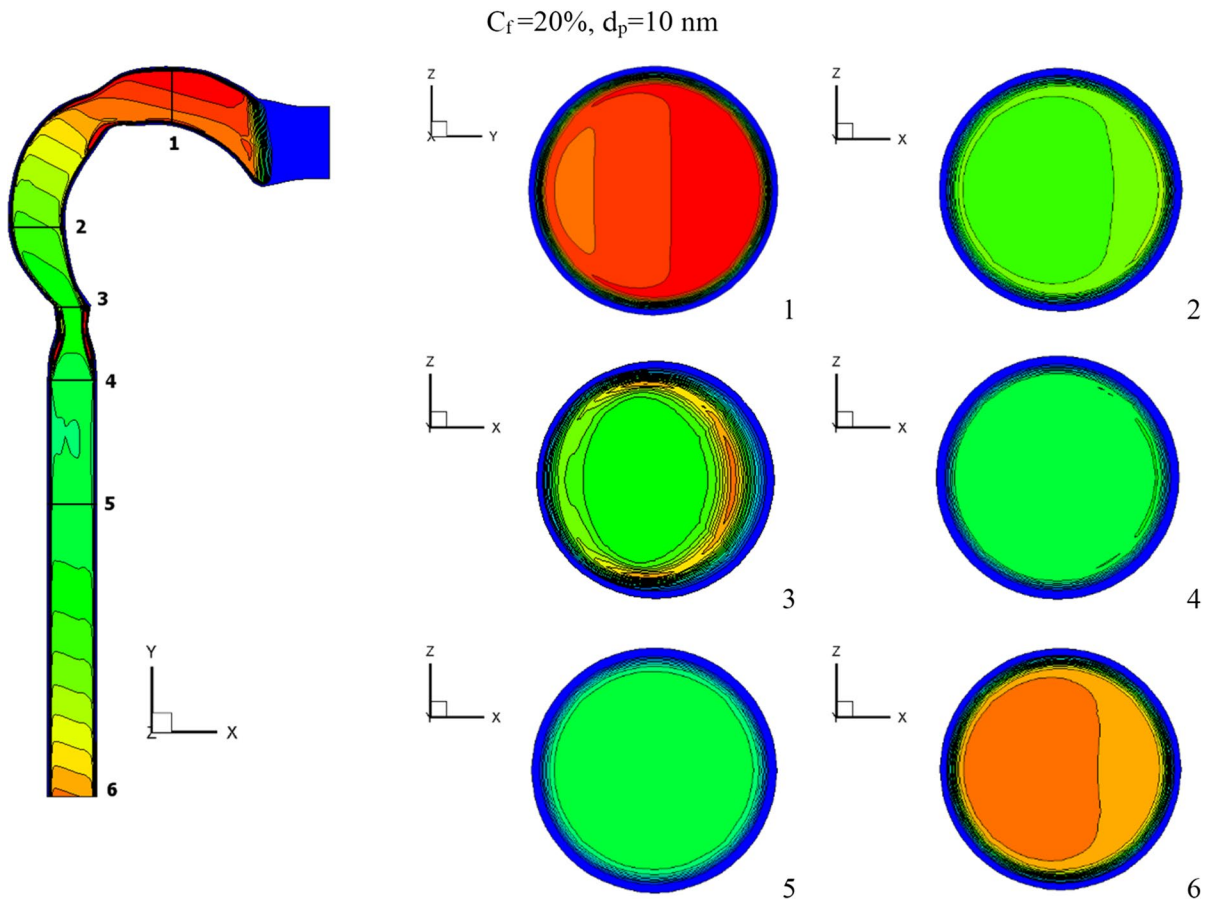

Fig. 12 (continued)

- The chlorine velocity rises in the pharynx/larynx at low chlorine mass fractions (2%) and inhalation rates of $Q = 15$ l/min and $Q = 30$ l/min.
- The volume fraction of chlorine reduces as the chlorine concentration (2%) falls and the breathing rate lowers.
- At a low breathing rate ($Q = 15$ l/min), lower chlorine particle diameter (10 nm), and lower chlorine mass fraction (2%), the maximum chlorine transmission distance approaches the oral cavity.
- The particles are accelerated to escape into the bronchial tubes at a high respiratory flow rate of 60 l/min, depending on the diameter of the chlorine particles (10 nm, 20 nm, 30 nm, and 50 nm) and the chlorine mass fraction (2%).
- At $Q = 15$ l/min and a diameter of 10 nm, the high chlorine mass fraction generates high velocity of chlorine particles, with average velocities of 2.7 m/s, 0.62 m/s, and 0.31 m/s, respectively, when the chlorine mass fraction is 20%, 15%, and 10%.
- As the mass fraction of chlorine increases, the turbulent kinetic energy in the outlet airway increases. The mean turbulent kinetic energy at the airway's exit is 14.4% and 2.2% greater at 20% chlorine than at 10% and 15% chlorine, respectively.
- When compared to $Q = 15$ l/min at a chlorine mass fraction of 20%, the deposition efficiency of $Q = 60$ l/min and $Q = 30$ l/min increases by around 21.8% and 4.1%, respectively.

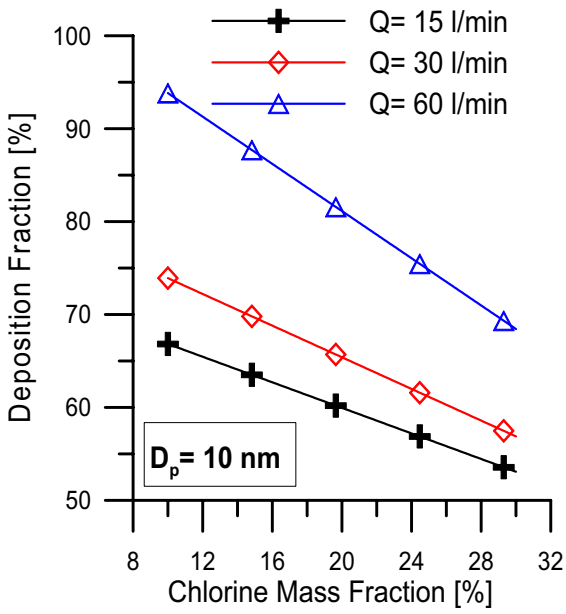

Fig. 13 Deposition fraction of chlorine in airway with different inhalation flow rates

Funding Open access funding provided by The Science, Technology & Innovation Funding Authority (STDF) in cooperation with The Egyptian Knowledge Bank (EKB).

Declarations

Conflict of interest The authors declare no competing interests.

Open Access This article is licensed under a Creative Commons Attribution 4.0 International License, which permits use, sharing, adaptation, distribution and reproduction in any medium or format, as long as you give appropriate credit to the original author(s) and the source, provide a link to the Creative Commons licence, and indicate if changes were made. The images or other third party material in this article are included in the article's Creative Commons licence, unless indicated otherwise in a credit line to the material. If material is not included in the article's Creative Commons licence and your intended use is not permitted by statutory regulation or exceeds the permitted use, you will need to obtain permission directly from the copyright holder. To view a copy of this licence, visit http://creativecommons.org/licenses/by/4.0/.

References

Bernstein GM (2004) A review of the influence of particle size, puff volume and inhalation pattern on the deposition of cigarette smoke particles in the respiratory tract. Inhalation Toxicol. 16: 675–689. https://doi.org/10.1080/08958370490476587

Breitner S, Liu LQ, Cyrys J, Brüske I, Franck U, Schlink U, Leitte AM, Herbarth O, Wiedensohler A, Wehner B, Hu M, Pan XC, Wichmann HE, Peters A (2011) Sub-micrometer particulate air pollution and cardiovascular mortality in Beijing, China. Sci Total Environ 409: 5196–5204. https://doi.org/10.1016/j.scitotenv.2011.08.023

Chalupa DC, Morrow PE, Oberdörster G, Utell MJ, Frampton MW (2004) Ultrafine particle deposition in subjects with asthma. Environ Health Perspect 112(8):879–882. https://doi.org/10.1289/ehp.6851

Chauhan S, Chauhan S, D'Cruz R, Faruqi S, Singh KK, Varma S, Singh M, Karthik V (2008) Chemical warfare agents. Environ Toxicol Pharmacol 26(2):113–22. https://doi.org/10.1016/j.etap.2008.03.003

Chen RJ, Li Y, Ma YJ, Pan GW, Zeng G, Xu XH, Chen BH, Kan HD (2011) Coarse particles and mortality in three Chinese cities: the China Air Pollution and Health Effects Study (CAPES). Sci Total Environ 409:4934–4938. https://doi.org/10.1016/j.scitotenv.2011.08.058

Chen H, Kwong JC, Copes R, Tu K, Villeneuve PJ, van Donkelaar A et al (2017) Living near major roads and the incidence of dementia, Parkinson's disease, and multiple sclerosis: a population-based cohort study. Lancet 389:718–726. https://doi.org/10.1016/s0140-6736(16)32399-6

Chen RJ, Kan HD, Chen BH, Huang W, Bai ZP, Song GX, Pan GW (2012) Association of particulate air pollution with daily mortality: the China Air Pollution and Health Effects Study. Am J Epidemiol 175(11): 1173–1181. https://doi.org/10.1093/aje/kwr425

Cheng KH, Swift DL (2016) Calculation of total deposition fraction of ultrafine aerosols in human extra thoracic and intrathoracic regions aerosol. Sci Tech 22:194–201. https://doi.org/10.1080/02786829509508887

Cheng YS, Yamada Y, Yeh HC, Swift DL (1988) Diffusional deposition of ultrafine aerosols in a human nasal cast. J Aerosol Sci 19:741–751. https://doi.org/10.1080/02786826.2010.488256

Cheng KH, Cheng YS, Yeh HC, Swift DL (1997) "Measurements of airway dimensions and calculation of mass transfer characteristics of the human oral passage", J. Biomech. Eng. – Trans. ASME 119:476–482. https://doi.org/10.1115/1.2798296

Cohen AJ, Brauer M, Burnett R, Anderson HR, Frostad J, Estep K, et al. (2017) Estimates and 25-year trends of the global burden of disease attributable to ambient air pollution: an analysis of data from the Global Burden of Diseases Study 2015. Lancet 389, 1907–1918. https://doi.org/10.1016/s0140-6736(17)30505-6

Cui XG, Gutheil E (2017) Three-dimensional unsteady large eddy simulation of the vortex structures and the monodisperse particle dispersion in the idealized human upper respiratory system. J Aeroso Sci 114:195–208. https://doi.org/10.1016/J.JAEROSCI.2017.09.005

Cui XG, Gutheil E (2018) Large eddy simulation of the poly-disperse particle deposition in an idealized mouth-throut. At Sprays 28(2):179–193. https://doi.org/10.1615/AtomizSpr.2018025127

Donaldson K, Stone V, Gilmour PS, Brown DM, Macnee W (2000) Ultrafine particles: mechanisms of lung injury. Philos Trans R Soc 358:2741–2749. https://doi.org/10.1098/rsta.2000.0681

Frampton MW (2001) Systemic and cardiovascular effects of airway injury and inflammation: ultrafine particle exposure in humans. Environ Health Persp 109:529–532. https://doi.org/10.2307/3454664

Friedlander SK (2000) "Smoke, Dust and Haze, Fundamentals of aerosol dynamics," 2nd edn. Oxford University Press, New York

Ghalati PF, Keshavarzian E, Abouali O, Faramarzi A, Tu J, Shakibafard A (2012) Numerical analysis of micro-and nano-particle deposition in a realistic human upper airway. Comput Biol Med 42:39–49. https://doi.org/10.1016/j.compbiomed.2011.10.005

Heal MR, Kumar P, Harrison RM (2012) Particles, air quality, policy and health. Chem Soc Rev 41:6606–6630. https://doi.org/10.1039/c2cs35076a

Horemans B, Van Holsbeke C, Vos W, Darchuk L, Novakovic V, Fontan AC, De Backer J, Van Grieken R, De Backer W, De Wael K (2012) Particle deposition in airways of chronic respiratory patients exposed to an urban aerosol. Environ Sci Technol 46 (21): 12162–12169. https://doi.org/10.1021/es302755s

ICRP (1994) Human respiratory tract model for radiological protection," Elsevier Science Ltd., New York

Kan HD, London SJ, Chen GH, Zhang YH, Song GX, Zhao NQ, Jiang LL, Chen BH (2007) Differentiating the effects of fine and coarse particles on daily mortality in Shanghai, China. Environ Int 33(3): 376–384. https://doi.org/10.1016/j.envint.2006.12.001

Keith CH (1982) Particle size studies on tobacco smoke. Beitr Tabakforsch 11 (3): 123–131. https://doi.org/10.2478/cttr-2013-0506

Kelly JT, Asgharian B, Kimbell JS, Wong BA (2004) Particle deposition in human nasal airway replicas manufactured by different methods. Part II: Ultrafine particles. Aerosol Sci Technol 38: 1072–1079. https://doi.org/10.1080/027868290883432

Kim CS, Jaques PA (2004) Analysis of total respiratory deposition of inhaled ultrafine particles in adult subjects at various breathing patterns. Aerosol Sci Technol. 38, 525–540. https://doi.org/10.1080/02786820490465513

Kittelson DB (1998) Engines and nanoparticles: a review. J Aerosol Sci 29(5–6):575–588. https://doi.org/10.1016/S0021-8502(97)10037-4

Kleinstreuer C, Zhang Z (2003) Laminar – to- turbulent fluid particle flows in a human airway model. Int J Multiphase Flow 271–289. https://doi.org/10.1016/S0301-9322(02)00131-3

Kumar P, Goel A (2016) Concentration dynamics of coarse and fine particulate matter at and around signalized traffic intersections. Environ Sci.: Processes Impacts 18:1220–1235. https://doi.org/10.1039/C6EM00215C

Lelieveld J, Evans JS, Fnais M, Giannadaki D, Pozzer A (2015) The contribution of outdoor air pollution sources to premature mortality on a global scale. Nature 525, 367. https://doi.org/10.1038/nature15371

Li X, Yan C, Patterson RF, Zhu Y, Yao X, Zhu Y, Ma S, Qiu X, Zhu T, Zheng M, (2016) Modeled deposition of fine particles in human airway in Beijing, China. Atmos Environ 124:387–395. https://doi.org/10.1016/j.atmosenv.2015.06.045

Meng X, Ma YJ, Chen RJ, Zhou ZJ, Chen BH, Kan HD (2013) Size-fractionated particle number concentrations and daily mortality in a Chinese city. Environ Health Perspect 121:1174–1178. https://doi.org/10.1289/ehp.1206398

Oberdorster G (2001) Pulmonary effects of inhaled ultrafine particles. Int Arch Occup Env Health 74:1–8. https://doi.org/10.1007/s004200000185

Underwood E (2017) The polluted brain. Science 355:342–345. https://doi.org/10.1126/science.355.6323.342

White CW, Martin JG (2010) Chlorine gas inhalation: human clinical evidence of toxicity and experience in animal models. Proc Am Thorac Soc 7: 257–263. https://doi.org/10.1513/pats.201001-008sm

Zhang Z, Kleinstreuer C (2003) Low Reynolds number turbulent flows in locally constricted conduits: a comparison study. AIAA J 41:831–840. https://doi.org/10.2514/2.2044

Zhang Z, Kleinstreuer C (2004) Airflow structures and nanoparticle deposition in a human upper airway model. J Comput Phys 198:178–210. https://doi.org/10.1016/j.jcp.2003.11.034

Publisher's note Springer Nature remains neutral with regard to jurisdictional claims in published maps and institutional affiliations.